ELASTO-PLASTIC BEHAVIOR OF REINFORCED CONCRETE BEAMS WITH SPANDREL WALLS UNDER ANTI-SYMMETRIC CYCLIC LOADS

by Yoichi Higashi[I], Masamichi Ohkubo[II] and Ken Iida[III]

SYNOPSIS

More than twenty of reinforced concrete beams with spandrel walls were tested to investigate the elasto-plastic behavior under anti-symmetric cyclic loads. The typical failure of the beams with spandrel walls were the flexural compression failure of spandrel wall and the diagonal shear failure. Remarkable stiffness and strength reduction occurred after the maximum strength in both failure patterns. The failure patterns were influenced by shear span ratio and ratio of shear reinforcement in the walls. Stiffness, flexural and shear strength and restoring force characteristics before and after flexural failure were analyzed and compared with the test results.

INTRODUCTION

Many reinforced concrete buildings with spandrel walls were heavily damaged in 1968 TOKACHI-OKI EARTHQUAKE.[1] One of the effects of spandrel walls on frame is the concentration of the lateral shear force due to the restricting of lateral displacement for the columns connected with such walls, another is the increasing of stiffness and strength of a beam with spandrel walls itself. Many reinforced concrete buildings with such walls have been constructed in Japan, and the buildings, in which the above effects were out of consideration in the structural analysis, were damaged in TOKACHI-OKI EARTHQUAKE.

In our laboratory, these problems were taken up as an important theme on earthquake resisting design just after the earthquake, and the fundamental tests with the small frames had been made to investigate the influences of spandrel walls to the failure.[2),3),4)] In this paper, the test results of fifteen kinds of beams with spandrel walls, in which shear span ratio, arrangement of shear reinforcement, tension reinforcement ratio in beam and wall thickness were varied respectively, and one rectangular beam without wall under anti-symmetric cyclic loading, are reported and stiffness, flexural and shear strength and restoring force characteristics are discussed.

TEST PROGRAM

Test specimens

The test specimens, as shown in Fig. 1, are approximately one third full scale of the beams with spandrel walls which are used in ordinary school buildings in Japan. The variable elements of the specimens are shown in Table 1. Structural round bars SR24 (9ϕ, ${}_s\sigma_Y = 3880 kg/cm^2$) and deformed

I) Professor, Dr. Eng., Dep't of Architecture, Tokyo Metropolitan Univ.
II) Assistant, Dep't of Architecture, Tokyo Metropolitan Univ.
III) Graduate Student, Dep't of Architecture, Tokyo Metropolitan Univ.

bars SD35 (D10, $_s\sigma_Y$ = 4090kg/cm^2 and D16, $_s\sigma_Y$ = 3855kg/cm^2) were used as the longitudinal reinforcement in beams, and annealed steel wires (4ϕ, $_{ws}\sigma_Y$ = 2280kg/cm^2) were used as the stirrups and wall reinforcement. The ordinary mixed concrete consisted of portland cement, river sands and small size aggregates were used, and their compressive strength of 15 x 15 cm. cylinders were 150 ~ 203kg/cm^2 at beam tests.

The test setup and measurements

The test specimens were subjected to anti-symmetric loads as shown in Fig. 2. The displacements due to the rotation between both left and right gage-holders δ were measured. A divisor δ/ℓ , where ℓ is the distance between both supports, gives an average of rotation angles θ at both ends, and it is used as the deformation of the specimens in the followings. The strains of concrete and longitudinal reinforcement at both ends and the strains of shear reinforcement were measured by using wire strain gages.

The control systems of cyclic loading

Two different control systems CC and SC were adopted in this test. In the system CC, as shown in Table 1, the loadings until failure were divided to three or four steps, and three to ten times of cyclic loadings were made in each step. In the system SC, the specimens were failed by simply increasing loads after a cyclic loading in elastic range. Several times of cyclic loadings in small and large deformation ranges after the failure were made to investigate the hysteretic characteristics after the failure in each control system.

FAILURE PATTERNS AND HYSTERESIS CURVES

Flexural failure

No. 2 specimen (see Fig. 3 and Fig. 4) which had the only top spandrel wall was failed by FY pattern at the beam end where the spandrel wall was subjected to tension. Flexural cracking B, yielding of longitudinal wall reinforcement Y' and yielding of beam reinforcement in tension side Y were orderly occurred as shown in Fig. 3. The ultimate loads were higher with additional strength due to the tension wall reinforcement in comparison with the rectangular beam No. 1 shown by dashed line in Fig. 3. In the opposite compression end, yielding of tension reinforcement and crushing of compression wall didn't occurred. The hysteresis curves in this specimen had considerable ductility.

Fig. 5 and Fig. 6 show the typical FC pattern due to flexural compression failure of spandrel walls. The failure progress of FC pattern up to the maximum load was flexural cracking B, yielding of longitudinal wall reinforcement Y', inclined shear cracking in the spandrel walls Sw, development of those shear cracks into the beam stem SB, yielding of longitudinal beam reinforcement Y and compressive crushing of spandrel wall C. The average rotation angle θ_u was about 1/100 radian at the maximum load. This pattern was observed in many specimens. The stiffness and strength reduction occurred suddenly by the brittle compression failure of wall as shown in Fig. 5. However, the hysteresis curve in the new cyclic loadings after

ɔmpression failure of spandrel wall was similar to that of the rec-
lar beam No. 1 subjected to similar large deformation.

failure

Fig. 7 and Fig. 8 show the typical SD failure pattern due to the propa-
n of shear crack width which developed diagonally in the direction of
compression fibers. This failure pattern appeared in the cases where
atio of stirrup p_w and transverse wall reinforcement p_s were low. The
resis loops were unstable, and the stiffness reduced extremely in
c loading after the shear failure as shown in Fig. 7. FSD pattern in
1 shows the diagonal shear failure after crushing of spandrel wall.

In SW pattern, which appeared in the case where p_s was few in spite of
p_w, the shear failure occurred in only spandrel walls. The stiffness
:tion after shear failure was smaller than that of SD pattern, because
r damage on the beam stem didn't occurred in even large deformation as
ı in Fig. 9 and Fig. 10.

DISCUSSION

fness and flexural cracking strength

The comparisons of the calculated stiffness in elastic range with the
results are shown in Table 1. The flexural deformation δ_B and the
r deformation δ_s obtained from Eq. (1) are considered in the calcula-
of stiffness.

$$\delta_B = Q\ell^3/12EI_o, \quad \delta_s = KQ\ell/GA \qquad \text{..... (1)}$$

·e, Q; shear force, ℓ; distance between both supports, E; Young's modulus
:oncrete ($E = 2.1 \times 10^5 \times (\gamma/2.3)^{1.5} \times \sqrt{F_c/200}$, kg/cm²), γ; density, Fc; com-
ssive strength, I_o; inertia moment for full cross-section neglecting the
:ct of reinforcement, K; shearing shape coefficient obtained from the
ıod of shear strain energy, G; shear rigidity of concrete $G = E/2(1+\nu)$,
'oisson's ratio, A; area of full cross-section neglecting the effect of
ıforcement. The ratios of the calculated stiffness to the tested were
veen 0.72 and 1.81, and the average of them was 1.12.

The comparisons of the flexural strength, obtained from Eq. (2), with
test results are also given in Table 1.

$$M_c = 1.8\sqrt{F_c} \cdot Z \qquad \text{..... (2)}$$

re, Z; modulus of section neglecting the effect of reinforcement for full
ss-section. The calculated strength agreed well with the test results
shown in Table 1, where the average for the ratios of calculation to test
0.99.

imate flexural strength

Fig. 11 shows the relation between shear force Q and longitudinal
·ain ε, and the strain distributions at the end section as an example of

tern. The yielding of lower beam reinforcement in tension side occur- about 2.4 ton, and the beginning of compression failure of concrete ·ed at about 3 ton. The load increased further until compression fai- ›f spandrel wall in spite of the yielding of lower beam reinforcement, ;e the tension force of upper beam reinforcement could increased as by $_s\varepsilon_2$ in Fig. 11. However, the yielding of lower beam reinforcement : occurred in No. 5b-1 and No. 5b-2 specimen, in which much beam re- :ement were provided.

Jltimate flexural strength based on the compression failure of concrete ındrel wall was calculated. The simplified cross-section was used as in Fig. 12 in which the effect of longitudinal wall reinforcement in ɜssion side was neglected and the followings were assumed.

Usual rectangular method was adopted, and the coefficient k_1, k_2, k_3 ɜ stress block of compressive concrete shown in Fig. 12 were assumed 0.8, 0.44 and 0.85, respectively.[5)]

The ultimate strain of concrete at compression fiber $_c\varepsilon_u$ was assumed 0.4%. According to the measurement of strains, $_c\varepsilon_u$ at compression of spandrel wall were between 0.2 to 0.6%, and the average of them .36%.

The linear distribution of strains, namely Bernoulli-Euler assumptions, ssumed by using the apparent strain of beam tension reinforcement $_s\varepsilon_1/F$ ε_2/F as shown in Fig. 12, because the reduction of bond stress was con- ·ed. The coefficient F, proposed by A.L.L. Baker[6)], was assumed to be .n this paper, because the values obtained from the test results were ; 0.2 to 0.6.

Using above assumptions and the notations shown in Fig. 12, the balanc- :eel ratio p_{t1b}, in which the yield strain of lower beam reinforcement and the ultimate strain of fiber concrete $_c\varepsilon_u$ occur simultaneously, is ı by Eq. (3),

$$p_{t1b}=(a_{t1}+\Sigma_w a_t\cdot {}_w\sigma_Y/{}_s\sigma_Y)/bD=k_1k_3F_c\cdot t\cdot x_{nb}/\{{}_s\sigma_Y+\gamma\cdot{}_c\varepsilon_u\cdot F\cdot{}_sE(d_o-x_{nb}-g)/x_{nb}\}bD \quad \ldots (3)$$

ɜ, the distance between neutral axis and compression fiber is given by (4),

$$x_{nb}=d_o\cdot{}_c\varepsilon_u/({}_s\varepsilon_Y/F+{}_c\varepsilon_u) \quad \ldots (4)$$

mate moment M_u is given by Eq. (5) and Eq. (6) in case of the yielding ower beam reinforcement, namely $p_{t1}\leq p_{t1b}$,

$$M_u=p_{t1}\cdot bD\{{}_s\sigma_Y(d_o-k_2x_n)+\gamma\cdot{}_c\varepsilon_u\cdot F\cdot{}_sE(d_o-x_n-g)(d_o-k_2x_n-g)/x_n\} \quad \ldots (5)$$

$$x_n=\frac{({}_s\sigma_Y-\gamma\cdot{}_c\varepsilon_u\cdot F\cdot{}_sE)\left[1+\sqrt{1+\{4k_1k_3F_c\cdot t\,\gamma\cdot{}_c\varepsilon_u F\cdot{}_sE(d_o-g)/p_{t1}\cdot bD({}_s\sigma_Y-\gamma\cdot{}_c\varepsilon_u\cdot F\cdot{}_sE)^2\}}\right]}{(2k_1k_3\cdot F_c\cdot t)/(p_{t1}\cdot bD)} \quad \ldots (6)$$

is given by Eq. (7) and Eq. (8) in case of no yielding of lower beam ıforcement, namely $p_{t1}>p_{t1b}$,

$$M_u=p_{t1}\cdot bD\cdot{}_c\varepsilon_u\cdot F\cdot{}_sE\{(d_o-x_n)(d_o-k_2x_n)+\gamma(d_o-x_n-g)(d_o-k_2x_n-g)\}/x_n \quad \ldots (7)$$

$$x_n = \frac{-{}_c\varepsilon_u \cdot F_s E(1+r)\left[1-\sqrt{1+\{4k_1k_3F_c t(d_o+rd_o-rg)/p_{t1}bD\,{}_c\varepsilon_u F_s E(1+r)^2\}}\right]}{(2k_1k_3F_c t)/(p_{t1}bD)} \quad \ldots (8)$$

The calculated values were compared with the test results in Table 1. The ratios of the calculated values to the tested values were between 0.87 and 1.21. The average of them was 0.98, and considerably good agreement was observed between the analysis and the test results. However, the modification of above equations shall be necessary for the beams in which the depth of compression wall becomes smaller and the neutral axis exists in beam stem, because the total force of compression concrete will vary from above equations.

Cracking and ultimate shear strength

In almost specimens, shear cracks occurred, and several specimens with small shear span ratio and low shear reinforcement failed by shear in the whole member or only in spandrel walls as described before. Fig. 13 shows the relation between average shear stress at cracking and shear span ratio. The top and bottom solid lines represent minimum and mean values, respectively, which were proposed by T. Arakawa.[7] The dashed line represents the nominal shear stress at cracking specified by ACI 318-71,[8] and increasing coefficient as deep beams is applied when M/Qd is smaller than one. These lines are those for rectangular beams, and not for beams with thin spandrel walls. However, in this paper, the test results were modified as following, and were compared with these lines. Namely we defined nominal shear stress τ_c as given in Eq. (9), and shear span ratio M/Qd_o as shown in Fig. 14 using the substituted rectangular beams, whose area was equivalent to original cross-section.

$$\tau_c = Q_c / b'j \quad \ldots\ldots\ldots (9)$$

where, Q_c; shear force at cracking, b'; width of substituted rectangular section, $j = 7d_o/8$, d_o; effective depth used in the calculation of ultimate flexural strength. The nominal shear stresses when first cracking arised in region of the beam wall connections and when above shear cracks developed into the beam stem are plotted by the marks of ○ and ● respectively in Fig. 13. It is observed that the test results comparatively correspond to two solid lines.

Fig. 15 shows the relation between the nominal shear stress at ultimate load and the shear span ratio. Two solid lines, proposed by T. Arakawa, and the dashed line specified by ACI 318-71 each for ultimate shear strength are also represented. The test results plotted by the marks of ● and ○ , which represent shear failure and flexural failure respectively, are modified by the substituted rectangular beams shown in Fig. 14. They are almost plotted in the zone over the minimum equation by T. Arakawa. However, we could not observed the clear tendency between τ_u and M/Qd_o, because the specimens failed by shear were not so many and were limited only to small shear span ratio.

According to the measured strains of shear reinforcement in the specimens failed by shear, the yieldings of almost transverse reinforcements in walls and stirrups, which crossed the diagonal between both compression fibers, were observed until maximum loads. These strain measurements and the

crack patterns show that the transverse reinforcements in walls are especially effective as shear reinforcement. Although the stirrups are effective only in region of midspan as shear reinforcement at first, those at the end of beam are effective as not only shear reinforcement but also the prevention of flexural failure of beam after the compression failure of walls.

Restoring force characteristics

Fig. 16 shows the envelope curves for positive loading in each specimen. The dashed tri-linear lines represent the Q-θ relations calculated by using Eq. (1) ~ (8) for stiffness in elastic range, flexural cracking strength and ultimate flexural strength, and using the stiffness reduction ratio in plastic range α_y given in Eq. (10).

$$\alpha_y = (0.043 + 1.64\, n\, p_t + 0.043\, M/Qd + 0.33\, \eta_o)(d/D)^2 \qquad \cdots\cdots (10)$$

where, n; ratio of Young's modulus of steel to concrete, p_t; ratio of longitudinal tension reinforcement, M/Qd; shear span ratio, η_o; ratio of axial stress to compressive strength of concrete, d; effective depth, D; full depth.

Eq. (10) is an empirical expression developed by S. Sugano[9] for many rectangular beams and columns of his investigation and others', whose M/QD is larger than two. Therefore, the substituted rectangular cross-section (b' x d_o) as shown in Fig. 14 were adopted to apply Eq. (10) to the beams with spandrel walls. As shown in Fig. 16, the calculated tri-linear lines approximately corresponded to the test results until failure, except for the specimens failed by shear. However, the study on limit of inelastic deformation are important as further problems, because the remarkable strength reduction occurred after flexural compression failure in these member as shown in Fig. 5. The ductility factors, defined as the ratio of deformation at the maximum load to the calculated yielding deformation, were 0.98 ~ 2.2 for flexural failure and 0.33 ~ 1.3 for shear failure.

The hysteresis curves in small and large deformation ranges after compression failure in wall show similar Q-θ relationships as that of rectangular beam without spandrel walls, as shown in Fig. 5. Therefore, the restoring force characteristics of the beams with spandrel walls for the case of flexural failure could be represented by two envelope curves, the virgin envelope curve up to failure shown in Fig. 16 and the other similar to the rectangular beam after the failure of spandrel walls.

Fig. 17 shows the relation between equivalent viscous damping constant h_e, based on the areas of loops in cyclic loading, and cycle number of loading at each deformation range. The left and right figure represent before failure and after failure, respectively. In the loading before failure, the hysteresis loops become stable by almost five times of cyclic loading, and h_e are being constant about 0.04 ~ 0.08. In the loading after failure, on the other hand, h_e are about 0.1 and appreciably larger than those before failure, although they have considerable dispersion. However, we could not observed the remarkable effects of deformation range and failure modes on h_e.

CONCLUSIONS

The behavior up to failure of reinforced concrete beams with spandrel wall is very complicated, and their failure modes and restoring force characteristics are influenced by the ratio of shear reinforcement in spandrel walls. In case of low shear reinforcement ratio and small shear span ratio, the diagonal shear failure propagating into whole member would occur, and in case of flexural failure the spandrel wall in compression side would be crushed deeply from compression fiber to the beam wall connection. The stiffness reduction and strength reduction due to failure are very remarkable in either failure pattern.

The calculated stiffness in elastic range and flexural cracking strength obtained from Eq. (1) and Eq. (2) for the full cross-section with spandrel wall, would be comparatively close to the test results, and Eq. (3) ~ Eq. (8) based on usual bending theory for rectangular beam, could be applied to estimate flexural ultimate strength.

As for shear strength the substituted rectangular beam instead of beam with spandrel walls could be applied to usual empirical equations.

The restoring force characteristics in flexural failure could be represented by virgin envelope curve up to failure and the envelope curve for the rectangular beam without walls after failure. However, the studies on the deformation limit of virgin envelope curve are important problems in future.

REFERENCES

1) "GENERAL REPORT ON THE TOKACHI-OKI EARTHQUAKE OF 1968", KIGAKU PUBLISHING Co., Ltd.

2) Y. Higashi, M. Ohkubo and H. Eto, "Cracks and Hysteresis of Reinforced Concrete Frames with Spandrel Walls", No. 169, Trans. of A.I.J.(Architectural Institute of Japan), March 1970.

3) Y. Higashi and M. Ohkubo, "Static and Dynamic Loading Tests of Reinforced Concrete Frames with Thin Spandrel or Wing Walls", Japan-U.S. Seminar on Earthquake Engineering of School Building, Sept. 1970.

4) M. Ohkubo, "Strength and Hysteresis of R. C. Frames with Spandrel or Wing Walls", No. 186, Trans. of A.I.J., Aug. 1971.

5) E. Hognestad, "Fundamental Concepts in Ultimate Load Design of Reinforced Concrete Members", Journal of The A.C.I., June 1952.

6) A. L. L. Baker, "THE ULTIMATE-LOAD THEORY APPLIED TO THE DESIGN OF REINFORCED & PRESTRESSED CONCRETE FRAMES", Concrete Publications Ltd.

7) T. Arakawa, "Experimental Studies on Shear Strength of Reinforced Concrete Beam, Conclusions", No. 66, Trans. of A.I.J., Oct. 1960.

8) "Building Code Requirements for Reinforced Concrete (ACI 318-71)", American Concrete Institute.

9) S. Sugano, "Studies on Plastic Rigidities of R.C. Structures - Part 3", The Annual Meeting of Kanto-Branch of A.I.J., June 1968.

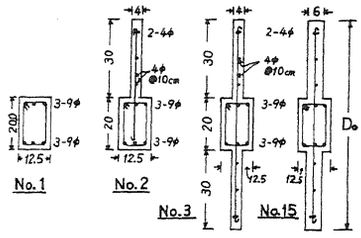

Fig. 1 - Test specimens

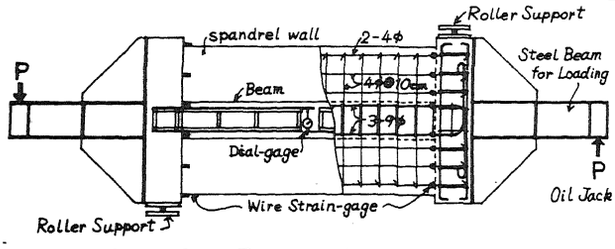

Fig. 2 - Test setup

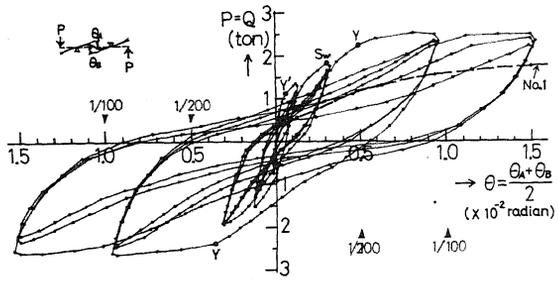

Fig. 3 - Load rotation relationships of No.2 specimen

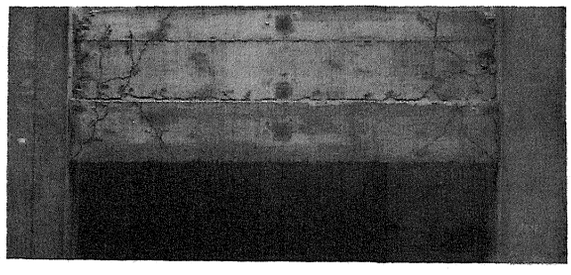

Fig. 4 - Crack pattern of FY-failure (No.2 specimen)

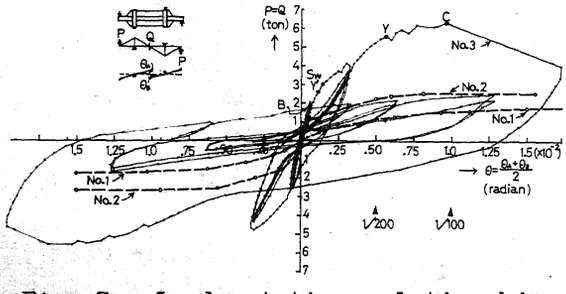

Fig. 5 - Load rotation relationships of No.3 specimen

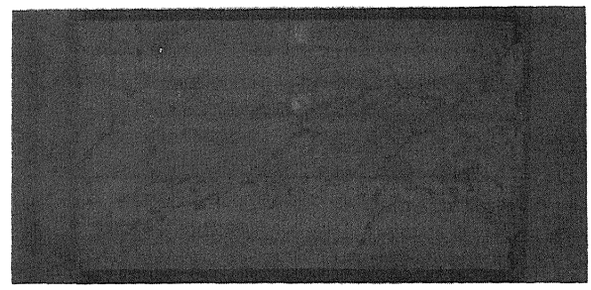

Fig. 6 - Crack pattern of FC-failure (No.3 specimen)

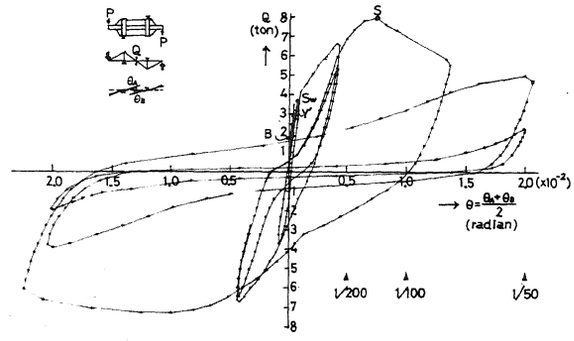

Fig. 7 - Load rotation relationships of No.9 specimen

Fig. 8 - Crack pattern of SD-failure (No.9 specimen)

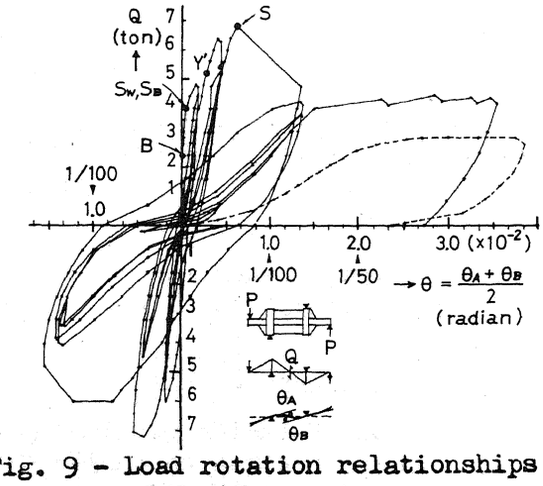

Fig. 9 - Load rotation relationships of No.12a specimen

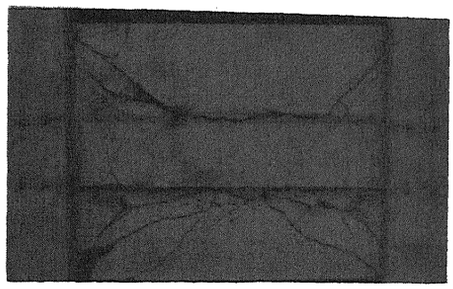

Fig. 10 - Crack pattern of SW-failure (No.12a specimen)

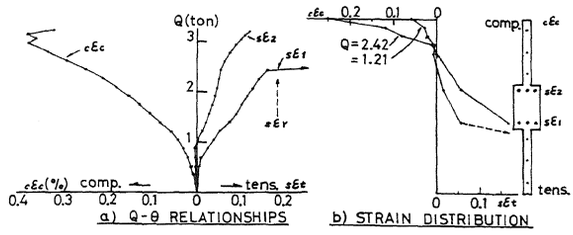

Fig. 11 - Measured strains of steel and concrete (No.8)

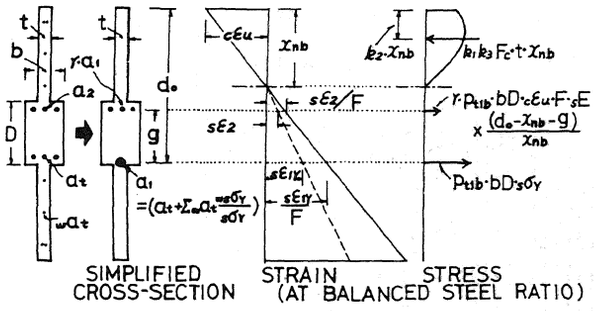

Fig.12 - Assumptions in flexural analysis

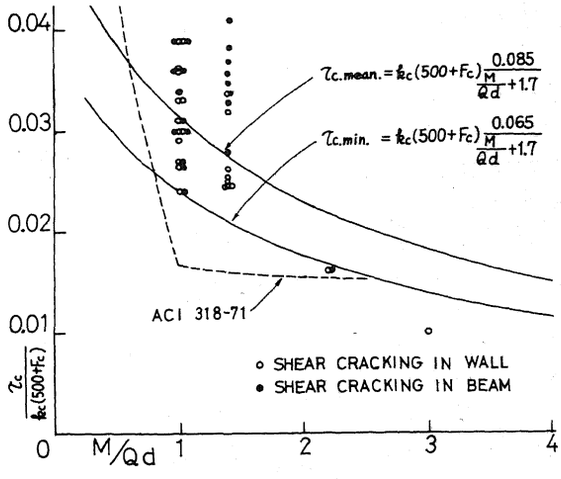

Fig. 13 - Relationships between τ_c and M/Qd

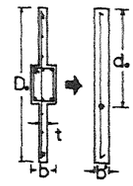

Fig.14 - Substituted cross-section

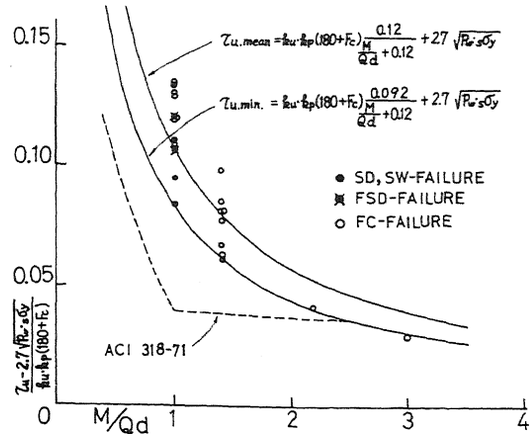

Fig. 15 - Relationships between τ_u and M/Qd

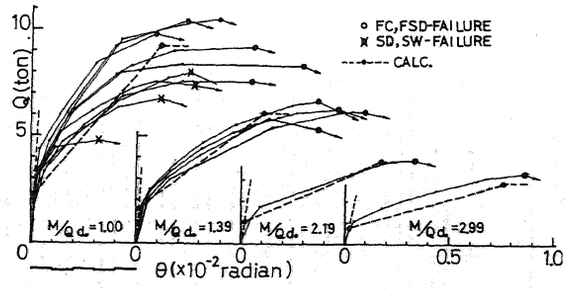

Fig. 16 - Envelope curves of load rotation relationships

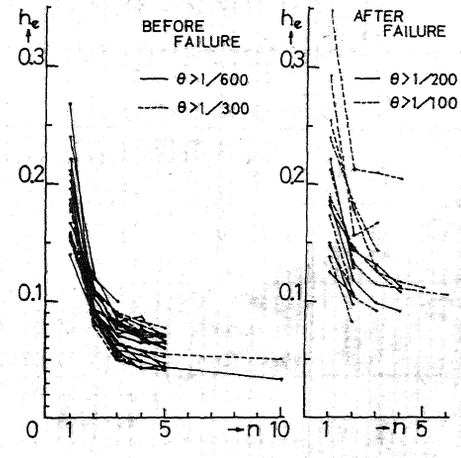

Fig. 17 - Relationships between h_e and n

Table 1 - Test results

No.	1) $\frac{M}{QD_o}$	2) p_w (%)	3) p_s (%)	4) p_t (%)	Loading system	Stiffness ($\times 10^3$ ton/radian) test	calc	calc/test	Cracking strength of flexure (ton) test	calc	calc/test	Ultimate strength of flexure (ton) test	calc	calc/test	5) Q_c (ton)	Q_u (ton)	6) θ_u ($\times 10^{-2}$ radian)	Mode of failure
1	3.50	0.20	-	0.77	CC	0.71	0.86	1.21	0.28	0.30	1.07	1.90	1.69	0.89	-	-	3.13	FY
2	1.40	0.20	0.31	0.77	CC	3.46	5.67	1.64	0.56	0.78	1.39	2.55	2.20	0.86	1.86	-	1.50	FY
3	0.875	0.20	0.31	0.77	CC	7,09	12.8	1.81	1.67	1.61	0.96	6.29	6.10	0.97	3.40	-	0.96	FC
4	0.875	0.40	0.31	0.77	CC	7.57	12.8	1.69	1.49	1.61	1.08	6.32	6.10	0.97	3.35	-	1.03	FC
5	0.875	0.20	0.62	0.77	CC	9.60	12.8	1.33	1.49	1.61	1.08	6.70	6.10	0.91	3.72	-	0.86	FC
5a-1	0.875	0.20	0.62	0.51	SC	11.4	11.6	1.02	1.63	1.60	0.98	4.78	5.06	1.06	3.38	-	0.74	FC
5a-2	0.875	0.20	0.62	0.51	CC	11.0	10.8	0.98	1.38	1.49	1.07	4.88	4.75	0.98	3.38	-	0.79	FC
5b-1	0.875	0.20	0.62	1.59	SC	13.6	10.1	0.74	1.63	1.38	0.85	6.17	5.90	0.96	4.13	-	0.79	FC
5b-2	0.875	0.20	0.62	1.59	CC	16.8	11.3	0.67	1.63	1.54	0.95	7.47	6.59	0.88	4.13	-	0.80	FC
6	0.875	0.40	0.62	0.77	CC	9.55	12.8	1.34	1.49	1.61	1.08	5.58	6.10	1.04	3.35	-	0.86	FC
7	1.375	0.20	0.31	0.77	SC	4.77	6.92	1.45	1.15	1.02	0.89	3.95	3.88	0.98	2.15	-	0.83	FC
8	1.875	0.20	0.31	0.77	SC	2.91	4.23	1.45	0.69	0.75	1.09	3.29	2.85	0.87	1.34	-	0.87	FC
9	0.625	0.20	0.31	0.77	CC	10.6	18.1	1.71	2.48	2.26	0.91	-	8.54	-	3.96	8.03	0.75	SD
10	0.625	0.20	0.31	0.85	SC	16.6	16.2	0.98	1.73	2.20	1.27	7.61	9.18	1.21	4.15	-	1.04	FSD
10a	0.625	0.20	0.31	0.85	CC	19.2	16.2	0.84	2.40	2.20	0.92	8.40	9.18	1.09	4.80	-	0.71	FSD
11	0.625	0.80	1.26	0.85	SC	22.6	16.2	0.72	2.00	2.20	1.10	9.80	9.18	0.94	4.40	-	0.59	FC
11a	0.625	0.80	1.26	0.85	CC	19.2	16.2	0.84	3.20	2.20	0.69	10.4	9.18	0.88	3.60	-	0.71	FC
12	0.625	0.80	0	0.85	SC	18.4	16.2	0.88	2.77	2.20	0.80	-	9.18	-	5.19	7.61	0.59	SW
12a	0.625	0.80	0	0.85	CC	16.7	16.2	0.97	2.40	2.20	0.92	-	9.18	-	4.00	6.80	0.63	SW
13	0.625	0	1.26	0.85	SC	22.1	16.2	0.73	2.08	2.20	1.06	9.26	9.18	0.99	4.84	-	1.05	FC
13a	0.625	0	1.26	0.85	CC	17.4	16.2	0.93	2.40	2.20	0.92	10.5	9.18	0.87	4.40	-	0.91	FC
14	0.625	0	0	0.85	CC	13.7	16.2	1.18	2.40	2.20	0.92	-	9.18	-	4.00	4.76	0.31	SD
15	0.625	0.20	0.21	0.85	CC	25.6	22.8	0.89	3.60	3.25	0.90	-	10.6	-	4.00	10.4	0.29	SD
16	0.625	0.80	0.84	0.85	CC	24.0	22.8	0.95	4.00	3.25	0.81	10.4	10.6	1.02	4.40	-	1.00	FC

1) Shear span ratio, D_o ; Beam depth plus height of spandrel walls, 2) $p_w = a_w/b \cdot s$, a_w; Area of a closed stirrup within a distance s, b; Beam depth, s; Spacing of stirrups, 3) $p_s = a'_w/t \cdot s'$, a'_w; Area of a transverse wall reinforcement within a distance s', t; Wall thickness, s'; Specing of wall reinforcement, 4) $p_t = a_t/b\,D$, a_t; Area of longitudinal beam reinforcement in tension side, D; Beam depth, 5) Shear strength in test, Q_c ; Cracking, Q_u ; Ultimate, 6) Rotation angle at failure, (radian).